# Comparison of effects from gamma, e-beam and X-ray radiation on multilayer polymer films used in biopharmaceutical devices by chemometric treatment of spectroscopic data

Blanche Krieguer, Sylvain R A Marque, Samuel Dorey, Fabien Girard, Yelin Ni, Donghui Li, Mark K Murphy, Leonard S Fifield, Nathalie Dupuy

Radiation Physics and Chemistry 218 (2024) 111607

Contents lists available at ScienceDirect

Radiation Physics and Chemistry

journal homepage: www.elsevier.com/locate/radphyschem

# Comparison of effects from gamma, e-beam and X-ray radiation on multilayer polymer films used in biopharmaceutical devices by chemometric treatment of spectroscopic data

Blanche Krieguer [a,b,c,*], Sylvain R.A. Marque [b], Samuel Dorey [a,**], Fabien Girard [c], Yelin Ni [d], Donghui Li [d], Mark K. Murphy [d], Leonard S. Fifield [d], Nathalie Dupuy [c,***]

[a] Sartorius Stedim FMT S.A.S, Z.I. Les paluds, Avenue de Jouques CS91051, 13781, Aubagne Cedex, France
[b] Aix Marseille Univ, CNRS, ICR, Case 551, 13397 Marseille, France
[c] Aix Marseille Univ, Avignon Univ, CNRS, IRD, IMBE, Marseille, France
[d] Pacific Northwest National Laboratory, Richland, WA 99354, USA

ARTICLE INFO

Handling Editor: Piotr Ulanski

*Keywords:*
FTIR
UV-VIS
Chemometrics
Gamma-ray
X-ray
e-beam

ABSTRACT

The present study investigated the effects of gamma-ray, electron beam, and X-ray radiation on polymers in EVA/EVOH/EVA multilayer films. Spectroscopic methods, including FTIR and UV–Vis, were employed in conjunction with chemometric treatments such as PCA, SIMPLISMA treatments, and PLS models. The feasibility of dose prediction on multilayer film, given a known dose, is attainable across various irradiation technologies. Both gamma ray and X-ray exhibit comparable effects on the multilayer film, and it is feasible to anticipate the dose released on the film by utilizing UV–Vis spectra or infrared spectra for gamma ray or X-ray of a predetermined dose.

## 1. Introduction

In a wide range of industrial sectors, including the production of single-use systems with multilayer plastic film for biopharmaceutical applications, gamma sterilization is utilized as a necessary and standardized process. Due to its extremely low residual toxicity, radiation sterilization offers a considerable benefit. Alternative irradiation technologies have emerged (Armenante and Akiti, 2019; Darwis et al., 2015; Dupuy et al., 2022; Komolprasert, 2016; Moondra et al., 2018), including electron beam (e-beam) and X-ray, despite the long history of gamma irradiation in the sterilizing process.

Polymers are used in a variety of medical and pharmaceutical products (Valente et al., 2016), including consumable plastic bags, gloves, and syringes. E-beam and X-ray sterilization are becoming more and more popular and numerous studies on the impact of this sterilization on medicinal goods, have been conducted since the technologies have become commercially available.

Previous studies have extensively examined the effects of gamma irradiation on EVOH and EVA polymers (Dinesh and Chikkakuntappa, 2013; Ji et al., 2019), while only a few studies have investigated the effects of e-beam and X-ray irradiation (Ahmed et al., 2020; Entezam et al., 2017; Matsui et al., 1992). Few studies have compared the effects of gamma and e-beam irradiation on EVA, with gamma irradiation having a greater impact on physical, mechanical, and thermal properties (Girard-Perier et al., 2022b). Other studies have compared the effects of gamma and electron beam irradiation on EVA shelf life, with no significant changes observed. Similarly, the effects of gamma and X-ray irradiation on the mechanical properties of EVA were found to be similar. For the EVA/EVOH/EVA multilayer film in this paper, various analytical techniques have been used to study the effects of gamma irradiation on different levels, but there is a lack of data on the effects of electron beam and X-ray irradiation on the spectroscopic properties of

* Corresponding author. Sartorius Stedim FMT S.A.S, Z.I. Les paluds, Avenue de Jouques CS91051, 13781, Aubagne Cedex, France.
** Corresponding author.
*** Corresponding author.
*E-mail addresses:* blanche.krieguer@sartorius.com (B. Krieguer), sylvain.marque@univ-amu.fr (S.R.A. Marque), samuel.dorey@sartorius.com (S. Dorey), fabien.girard@univ-amu.fr (F. Girard), yelin.ni@pnnl.gov (Y. Ni), donghui.li@pnnl.gov (D. Li), Mark.Murphy@pnnl.gov (M.K. Murphy), leo.fifield@pnnl.gov (L.S. Fifield), nathalie.dupuy@univ-amu.fr (N. Dupuy).

https://doi.org/10.1016/j.radphyschem.2024.111607
Received 13 June 2023; Received in revised form 18 December 2023; Accepted 11 February 2024
Available online 16 February 2024

multilayer materials. The use of ionizing irradiation as a sterilization method can cause bond cleavage and cross-linking, which may alter the physical and mechanical properties of the polymers. The chemical composition of polymers, the presence of additives, or the amount of oxygen in the surrounding environment all have an impact on polymers when exposed to radiation: radicals are created (Audran et al., 2015), the molecular weight of the polymer changes due to crosslinking, oxidized molecules are created, scission and other species like ions, excited macromolecules, etc (Darwis et al., 2015; Fifield et al., 2021; Matsui et al., 1992; Tarantili and Kiose, 2008).

The literature describes the cross-linking and chain scission events related to the effect of radiation on molecular weight distribution.

All these analyses (Driffield et al., 2014; Gaston et al., 2016a; Girard-Perier et al., 2022a; Tarantili and Kiose, 2008; Fifield et al., 2021) were performed on ready-to-use materials prepared in the factory and the several irradiations were performed in sterilization companies in classic industrial conditions. This approach has a strong limitation due to the non-controlled environment, which was circumvented by taking care on repeatability and reproducibility on the experiments.

In this study, an ethylene vinyl acetate (EVA)/ethylene vinyl alcohol (EVOH)/EVA multilayer film was analyzed after irradiation with gamma, X-ray, and e-beam in order to evaluate the effects of the three irradiation technologies on the film from a spectroscopic point of view.

A multilevel analytic approach is used for the investigation of EVA/EVOH/EVA multi-layer films: (i) analysis at the macromolecular level to get insights into the chemical changes leading to deterioration of material integrity by infrared spectroscopy (micro infrared and classic ATR/FTIR); and (ii) analysis at the molecular level to understand the behaviour of additive (antioxidants) by UV–Vis spectroscopy. Such approach generates a huge amount of data; thus, analyses of these data are performed using chemometrics methods such as Principal Component Analysis PCA and partial least square regressions (PLS). The goal of this study is to use infrared and UV–Vis spectroscopy to compare the effects of gamma, X-ray and e-beam radiation on multilayer films at various doses using the same unirradiated films as a reference. Quantitative models are built for each irradiation technology to predict the dose received. These models, once validated for an irradiation technology, are then used to predict the dose received for other irradiation technologies, in order to understand if the impact of the different irradiation technologies is similar.

## 2. Materials and methods

### 2.1. EVA/EVOH/EVA multilayer film and additives

The two batches of EVA single-use plastic bags investigated are made from a multilayer film composed of one layer of EVOH sandwiched between two layers of EVA, with a total thickness of approximately 360 μm. Sample bags are provided by Sartorius Stedim FMT S.A.S., Aubagne, France. Two different batches were examined in order to consider batch-to-batch variation. The different layers of these films contain additives such as antiblocking agents and antioxidants (AO) to stabilize them during the manufacturing process and during their shelf life.

### 2.2. Irradiation technologies

Precut EVA/EVOH/EVA samples were irradiated in gamma, e-beam and X-ray facilities. Samples were packed and wrapped in 100 ± 20 μm thick packaging films made of polyethylene (PE)/polyamide (PA)/PE during irradiation.

- Gamma irradiation

Gamma irradiation was carried out at room temperature with a cobalt-60 source at Ionisos (Dagneux, France) at a dose rate of 1–2 kGy $h^{-1}$. Co-60 has 1.17 and 1.33 MeV gamma energies. Multiple sterilization cycles were performed to obtain target doses. The waiting time between cycles and storage conditions were not specifically controlled. The actual delivered dose was measured using alanine dosimeters on a cardboard box (±5%). For the UV–Vis and ATR-FTIR analyze the doses delivered are 30, 44 and 61 kGy and for the micro-ATR FTIR the doses delivered are 30, 59 and 106 kGy.

- Electron beam irradiation

For the ATR-FTIR and UV–Vis spectroscopy, e-beam irradiation was performed using two 10 MeV, 20 kW Mevex accelerators at Steri-Tek (Fremont, California, USA), the dose rate being 18 MGy $h^{-1}$. The delivered doses are 31, 47 and 59 kGy for double sided irradiation.

Model B3 dosimeters were used on cardboard boxes to assess the radiation delivered to the film samples (±5%). For the micro-ATR-FTIR, e-beam irradiation was performed using a 10 MeV Rhodotron (Ionisos, Chaumesnil, France) with a power source at 28 kW, the dose rate being 18 MGy $h^{-1}$ (Chmielewski and Sun, 2017; Kroc, 2023). Alanine dosimeters were used on the cardboard to assess the radiation delivered (±5%) to the single-use bag samples. The delivered doses are 25 and 52 kGy for double sided irradiation.

•X-ray irradiation.

X-ray irradiation has been performed at Aerial-CRT on Feerix facilities. This facility is based on a Rhodotron (TT300 – IBA) and delivers X-ray beams. In this study, 7 MeV X-rays have been obtained from the conversion of 7 MeV electrons in a tantalum target. Irradiation has been performed with a vertical scan and a horizontal translation of products. The average dose rate was about 12 kGy $h^{-1}$. This, together with the adapted packaging of plastic parts in thin craft boxes, provides good treatment uniformity.

Delivered doses are 33, 45, 60 and 99 kGy ±10% for the UV–Vis and ATR-FTIR analysis and for the micro-ATR FTIR the delivered doses are 25, 50 and 100 kGy. The dose was verified by placing dosimeters in the cardboard box volume. Dosimetry has been performed using alanine.

### 2.3. Micro ATR FTIR

Micro-ATR-FTIR (μIR) is an extremely useful technique for confirming the identity of pure compounds (Voronko et al., 2014; Wrobel et al., 2015). The technique is based upon the identification of functional groups within molecules where such groups vibrations intensify through infrared radiation absorption (either through stretching torsion or bending in various ways). These vibrations and their intensity (reflectance) are plotted against the wavenumbers ($cm^{-1}$) to which the sample is exposed to produce an FTIR spectrum. Micro-ATR-FTIR makes it possible to analyze surfaces that are theoretically as small as the limit imposed by the diffraction of infrared radiation. Using the most powerful microscopes equipped with sophisticated optical systems and highly sensitive detectors, it is possible to analyze areas as small as 10 μm × 10 μm (Gardette, 1998). The obtain spectra are not saturated. The cross-section (Fig. 1) of each EVA/EVOH/EVA film sample was analyzed starting from the external face to the internal face. The set of spectra produced is called a mapping. The spectrometer used was a Thermo Nicolet Scientific MIR spectrometer with a microscope and ATR module, model IN10, with MCT detectors cooled with liquid nitrogen for better sensitivity. The spectrometer was placed in an air-conditioned room at 22 °C. Between each analysis, the KBr/Ge beam splitter was cleaned with an ethanol solution. At the beginning of each analysis, a reference spectrum was recorded, and the spectra were recorded with 16 scans and a resolution of 8 $cm^{-1}$. Each mapping was recorded in line form (Fig. 1) and the spectra were acquired every 10 μm. We did not consider spectra with too low signal-to-noise ratio; a total of 293 recorded spectra are available for chemometric analysis.

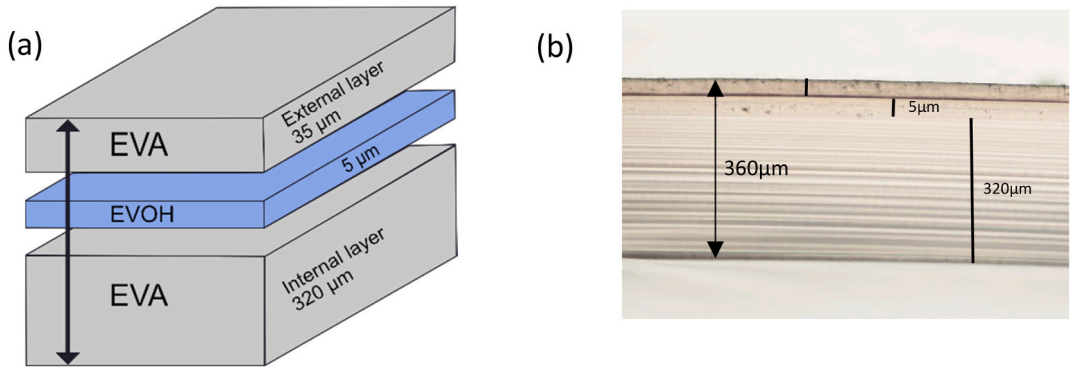


**Fig. 1.** (a) Representation of EVA/EVOH/EVA multilayer film; arrow represents the cross-section (b) microscopic image of cross-section of multilayer film.

### 2.4. ATR-FTIR

Fourier transform infrared spectroscopy (FTIR) was used to characterize chemical property changes on the polymer surface. After conditioning (23 °C and 50% relative humidity for at least 40 h), the samples were measured by Alpha II FTIR spectrometer (Bruker Corporation, MA, USA) with a diamond attenuated total reflection (ATR) crystal. The spectra of each sample were recorded from 4000 to 400 $cm^{-1}$ with 64 scans and a resolution at 4 $cm^{-1}$. For each sample, spectra were measured at four locations near the four edges of the sample. We did not consider spectra with too low a signal-to-noise ratio; a total of 220 recorded spectra are available for chemometric analysis.

### 2.5. Ultraviolet spectroscopy (UV–Vis)

UV–Vis spectroscopy is one of the most simple and economical methods for analysis of polymer film (Di Benedetto and Breuil, 2007; NicDaéid, 2018). UV–Vis transmittance from 200 nm to 800 nm was measured on a Cary 5000 UV–Vis–NIR spectrophotometer (Agilent Technologies, Inc.) with a solid sample holder. Three films irradiated at 30, 45, 60 kGy by gamma, e-beam and X-ray technologies were tested. Each film sample was tested three times. Prior to testing, the incident beam in the spectrometer was turned on for at least 30 min until it fully stabilized. Baseline scans (100% transmittance) were performed using the sample holder. Stabilization of the beam source was checked by examining the smoothness of the baseline.

### 2.6. Curve resolution method (SIMPLISMA)

The SIMPLe-to-use Interactive Self-modelling Mixture Analysis (SIMPLISMA) method, described in the literature (Gemperline, 1989; Hamilton and Gemperline, 1990; Windig, 1994, 1997; Windig and Stephenson, 1992; Windig and Guilment, 1991), was used for self-modelling mixture analysis by resolving mixture data into pure component signal and concentration profiles without the help of prior information about the mixture. Plastics are always a mixture of polymers and additives. SIMPLISMA will consider as “pure” either a mono-material or a mixture which evolves in a consistent way after irradiation (Gaston et al., 2018). When the radicals have the same kinetic trend and the same concentration profile, this tool is unable to differentiate the characteristics of different components. SIMPLISMA analysis is based on least squares optimization to determine the pure signal that has received the contributions from only one component. To properly handle noise, peak shifts, and instrument drift, user interactions are required (Audran et al., 2015).

The fitting of the SIMPLISMA results is calculated using the Relative Residual Sum of Squares (RRSSQ) (Windig, 1994), square sum between the calculated and the original spectra. The SIMPLISMA data treatments are performed with MATLAB 2009 software.

### 2.7. Principal Component Analysis (PCA)

Principal component analysis (PCA) is a tool commonly used in chemometrics (Kumar et al., 2014; Martens and Naes, 1989) and was described in a previous study (Audran et al., 2015). Each principal component (PC) is constructed to maximize the variance extracted from the remaining data. The projection of the scores in the space defined by the PCs gives an overview of the similarities and differences between the samples, while the loadings indicate which variables bring more information to each PC. In this study, we considered for each model only the PCs containing more than 15% of the variance. Thus, in some cases only the first PC was relevant, and the scores could be represented as a bar chart. In other cases, the first two PCs were relevant, and the scores could be represented as a scatter plot.

PCA was performed on spectra acquired in µIR on irradiated film EVA/EVOH/EVA by gamma, e-beam, and X-ray at 25, 50 and 100 kGy. To highlight the impact of the irradiation technology, only two ageing scenarios were selected (12 months for non-irradiated samples and 6 months). The spectra were corrected with a baseline and standard normal variate (SNV) pretreatment to correct for additive and multiplicative effects. PCA models were performed using CAMO (Computer Aided Modelling, Trondheim, Norway) software UNSCRAMBLER *X*.1.

### 2.8. Partial least square model (PLS)

Partial least squares (PLS) regression (Daszykowski et al., 2007; Ergon and Esbensen, 2002; Liang and Kvalheim, 1996; Martens, 1979; Sjöström et al., 1983) is a supervised method which is based on the relation between signal intensity (spectrum) and the characteristics of the sample (Y variable). Interference and overlapping information may be overcome by using a powerful multicomponent analysis such as PLS. The algorithm is based on the ability to mathematically correlate spectral data to a property or a concentration. PLS models were performed using CAMO (Computer Aided Modelling, Trondheim, Norway) software UNSCRAMBLER *X*.1.

## 3. Results and discussion

The modifications of the film after irradiation by gamma, e-beam and X-ray are analyzed on several scales: to the $cm^2$ with analysis in UV–Vis, to the $mm^2$ with analysis in infrared and to some $\mu m^2$ with analysis in µIR.

### 3.1. ATR-FTIR

The infrared spectra of the EVA/EVOH/EVA multilayer film non-irradiated and irradiated by gamma, e-beam, and X-ray doses ranging from 30 to 60 kGy displayed in Fig. 2. According to the literature (Gaston et al., 2016a), the main signal changes are observed in the

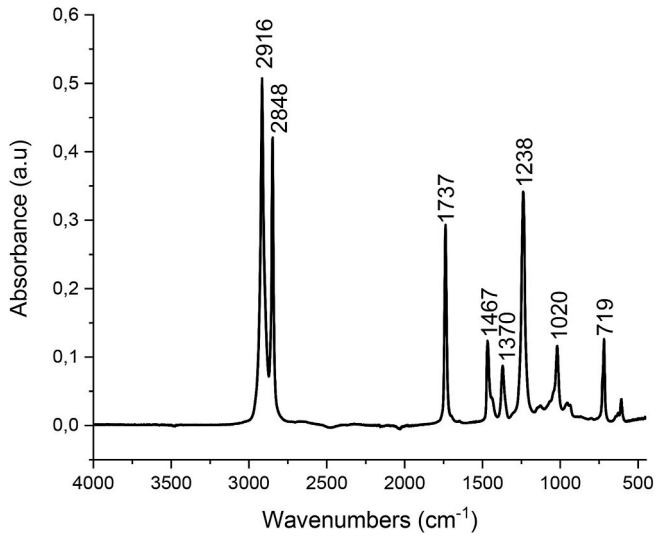


**Fig. 2.** Overlay of 220 EVA/EVOH FTIR spectra for non-irradiated samples.

carboxylic acid region (1737 $cm^{-1}$). The IR assignments of the EVA and EVOH spectra are given in Table S1 in accordance with the literature (Gaston et al., 2016a; Wool et al., 1986). The peak at 2916 $cm^{-1}$ corresponds to the antisymmetric stretching ($\nu CH_2$), the peak at 2848 $cm^{-1}$ corresponds to the symmetric stretching ($\nu CH_2$), and the peak at 1737 $cm^{-1}$ corresponds to the $\nu$CO of the ester. Peaks included between 1470 and 1360 $cm^{-1}$ correspond to the deformation in the plane of the $\delta CH_2$ and $\delta CH_3$ groups. Peaks included between 1300 and 1020 $cm^{-1}$ correspond to the stretching $\nu$CO, the peak at 730 $cm^{-1}$ (shoulder) corresponds to the inner rocking vibration of $CH_2$ in the crystalline part ($\delta CH_2$), and the peak at 719 $cm^{-1}$ corresponds to the inner rocking vibration of $CH_2$ in the amorphous part ($\delta CH_2$) (Gaston et al., 2016a).

### 3.1.1. Principal component analysis

The PCA displayed in Fig. 3 concerns the FTIR fingerprint spectral region [1800–700 $cm^{-1}$] and is performed on the 220 spectra representing the effects of all irradiation doses and technologies. For this region, the EVA spectra are baseline corrected and normalized. The first principal component (PC1) represents 52% of the total variance of the modification of the spectra. The second component (PC2) represents 22% of the total variance. In PCA approach, the data are clustered based on the similarities between samples by plotting two principal components relative to each other. All changes observed in PC1 and PC2 are correlated with the irradiation dose, regardless of the technology. Principal components (PCs) describe the variations among the objects in decreasing order, from the greatest to the smallest.

Fig. 3a displays then two different groups, the irradiated and the non-irradiated samples. Neither the effect of the different radiation technologies is visible, nor is the effect of the dose received at 30, 45 and 60 kGy. The first two components are the difference between the irradiated and non-irradiated spectra. Representation of variables PC1 and PC2 (Fig. 3b and c) highlight the wavenumbers contributing to the difference. No difference is observed on the investigated irradiation technologies.

When irradiated the primary signal change is noticeable in the carbonyl zone (1720-1740 cm-1). No signal changes are noticeable in the carboxylic acid zone (around 1714 cm-1) and the trans alkene zone (between 880 and 980 cm-1). The extent of these changes do not varies clearly depending on the absorbed dose with a different technologies, as shown in Fig. 3a and emphasized by the PCA. The peaks observed in the 730–700 cm-1 zone do not exhibit strong variation in the absorbed doses.

### 3.1.2. PLS regression

As the PCA showed that the unirradiated samples were slightly different from the irradiated samples, we quantified the dose received by those samples. A PLS regression was modeled to do so. The purpose of the PLS model is to extrapolate the effect of irradiation on the EVA/EVOH/EVA film to simulate the radiation dose received by the polymers regardless of the radiation source. We applied 3 PLS models, one for each irradiation technology.

Half of the non-irradiated samples and all samples irradiated at 30 and 60 kGy using gamma radiation were used for modelling. Samples irradiated at 45 kGy by gamma rays and half of the non-irradiated samples are used for prediction (Table S2). The modelling results ($R^2$ = 0.99, RMSEC = 1.52) show that a good correlation is obtained between the infrared spectra and the absorbed gamma radiation dose. The model was then used to predict the absorbed dose for samples irradiated by X-ray or e-beam at 30, 45 and 60 kGy (Fig. 4a). The results show that X-ray doses are correctly predicted while e-beam doses are underestimated.

A similar model was built for the X-ray irradiated samples. Half of the non-irradiated samples and all samples irradiated at 30 and 60 kGy using X-ray irradiation were used for modelling. Samples irradiated at 45 kGy by X-ray and half of the non-irradiated samples are used for prediction (Table S2 in SI). The modelling results ($R^2$ = 0.99, RMSEC = 1.94) show that a good correlation is obtained between the infrared spectra and the X-ray absorbed radiation dose. The model was then used to predict the absorbed dose for samples irradiated by Gamma or e-beam at 30, 45 and 60 kGy (Fig. 4a). The results show that gamma doses are correctly predicted while e-beam doses are underestimated.

A model was then built for the e-beam irradiated samples. Half of the non-irradiated samples and all samples irradiated at 30 and 60 kGy using e-beam were used for modelling. Samples irradiated at 45 kGy, and half of the unirradiated samples are used for prediction. The modelling results ($R^2$ = 0.99, RMSEC = 3.38) show that a good correlation is obtained between the infrared spectra and the received e-beam doses. The prediction results (Table S2) show that the model is applicable: non-irradiated samples are predicted with an average dose of 1 kGy, the dose of samples irradiated at 45 kGy by e-beam is predicted as 43.6 kGy. The model used to predict the absorbed dose for samples irradiated by gamma or X-ray at 30, 45 and 60 kGy show that X-ray doses and gamma doses are overestimated. Consequently, e-beam irradiation produces effects in different proportion on polymers than gamma and X-ray irradiation technologies, and the PLS models underestimate the expected dose for the electron beam. The gamma and the X-ray impact prediction are both in good agreement as they are both photon based technologies delivering doses in similar dose rate range. X-ray technology can deliver dose with dose rate <100 kGy $h^{-1}$ and gamma technology deliver dose with dose rate <10 kGy $h^{-1}$. E-beam technology can deliver dose with dose rate <30,000 kGy $h^{-1}$. We know according to ISO11137 that normally the higher the dose rate, the lower the impact on polymers without details on this statement. This could explain that e-beam production is not in agreement with the other ones.

The plot of the spectra (Fig. 5) displays that the effects of three irradiation technologies are different. The effect on the band at 720 $cm^{-1}$, which corresponds to the inner rocking vibration of $CH_2$ in the amorphous part ($\delta CH_2$) varies with the technology used. e-beam irradiation has a lesser effect on the crystallinity of the polymer compared to gamma and X-ray irradiation.

## 3.2. Micro infrared ($\mu$IR)

To complement the previous ATR study on the surface of the multilayer film, we analyzed the cross section of the film by μIR (Fig. 1). The aim of this analysis is to evaluate the effects inside the film and to conclude on the homogeneity of the film after irradiation with gamma, e-beam and X-ray.

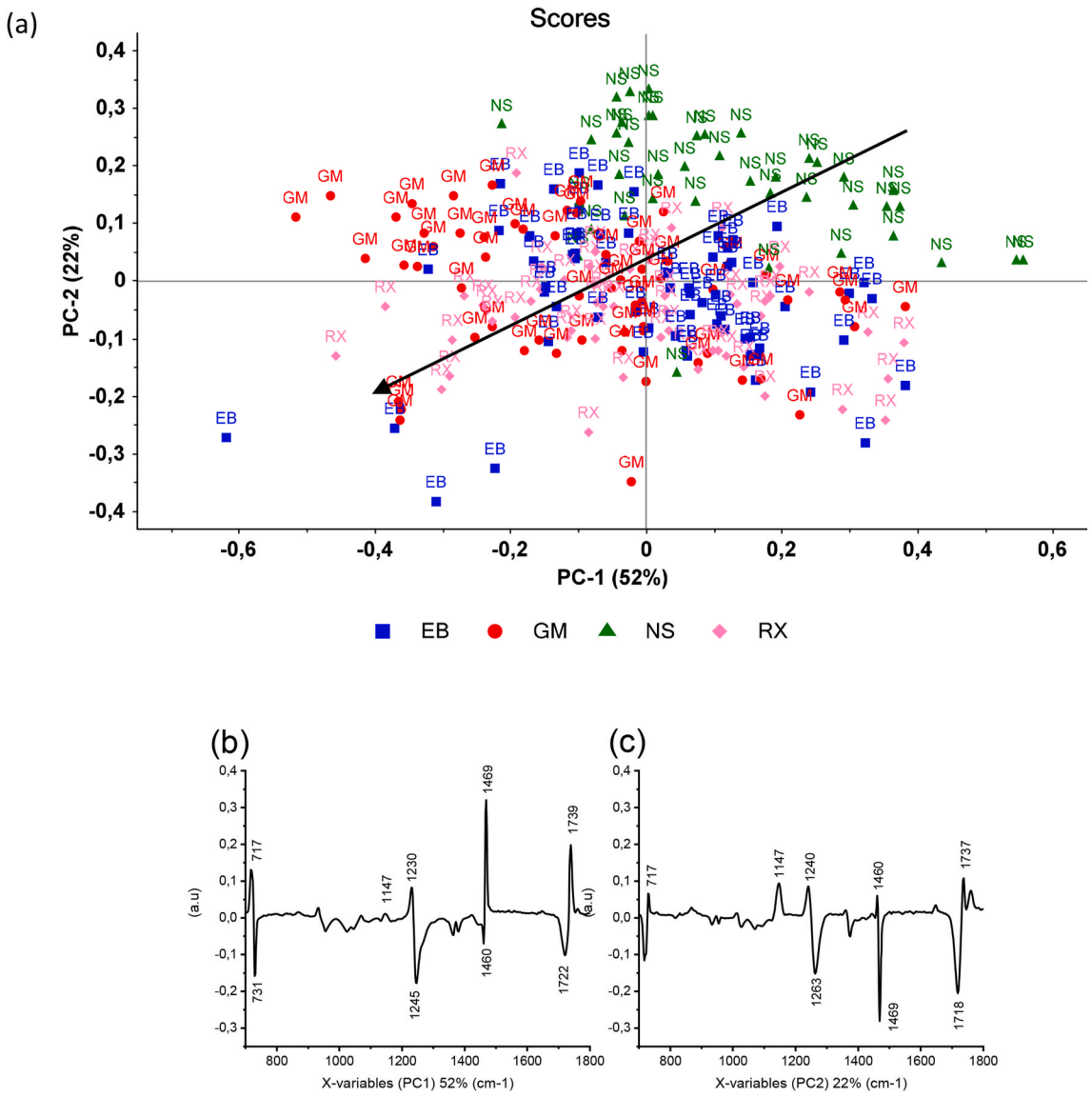


**Fig. 3.** PCA of 220 EVA spectra of non-irradiated and gamma, e-beam and X-ray irradiated samples at 30, 45 et 60 ± 10% kGy•h$^{-1}$. Spectra are baseline corrected and normalized. a) Score plot of PCA with irradiation technology (NS: non-irradiated, EB: e-beam irradiation, GM: gamma irradiation, RX: X-ray irradiation). (b) Loading plot of PC-1. (c) Loading plot of PC-2.

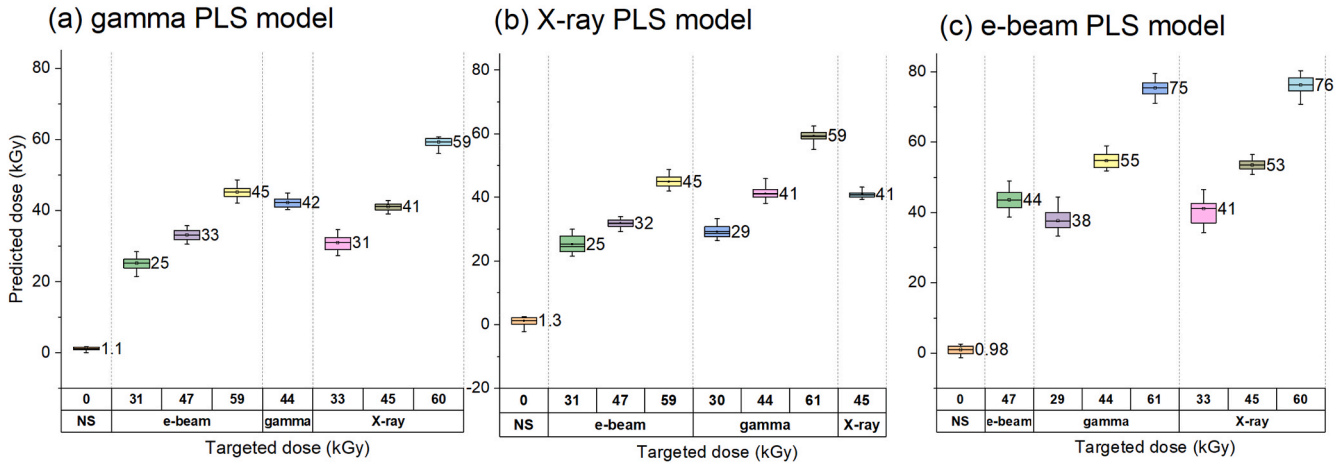


**Fig. 4.** PLS model using ATR spectra of (a) gamma irradiated samples. (b) X-ray irradiated samples. (c) e-beam irradiated samples. Labels correspond to predicted doses. Missing data were used to build models.

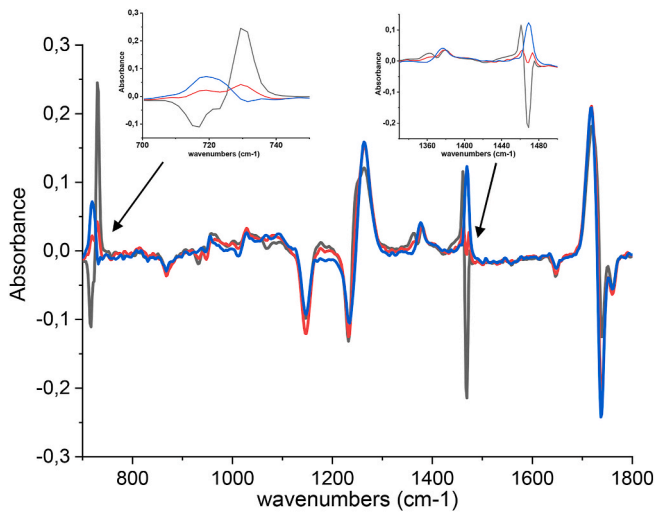


**Fig. 5.** Spectra representing model PLS (black line) with gamma irradiated samples, (red line) with X-ray irradiated samples and (blue line) with e-beam irradiated samples at 25, 50 and 100 kGy ± 10%.

### 3.2.1. PCA

The PCA displayed in Fig. 6 concerns the carbonyl and ester zones [1800–700 $cm^{-1}$] and is based on the 293 spectra measured on the cross-section, 6 months after irradiation for each dose and irradiation technology. The cross-section spectra are baseline corrected and normalized. The first principal component (PC1) represents 73% of the total variance of the modification of the spectra. The second component (PC2) represents 11% of the total variance.

Fig. 6 displays the PCA score, and the variable plot displays the μIR spectra of the main species present in the cross-section. The presence of oxidized EVA cannot be detected, as the acid peak at 1714 $cm^{-1}$ is not visible in the spectrum obtained after PCA. The intensity of the characteristic peak of the ester at 1739 and 1238 $cm^{-1}$ is high, so PC1 represents the pure EVA spectra. Similarly, it is not possible to detect the EVOH layer with this analysis method, the typical EVOH peak is the deformation of –OH peak at 1100 $cm^{-1}$. The PC1 score displays no effect of dose or irradiation technology. The samples are not grouped with their irradiation mode, or with the absorbed radiation dose of the film as no changes in the apparent cross-section of EVA layer after irradiation are observed. As the EVOH layer is not detected, only the score of the EVA spectra was analyzed. There would be no correlation between the doses or the irradiation technologies if the main species present in all spectra analyzed after irradiation are similar to those present before the irradiation. Detailed explanation of PCA could be find in reference (Gaston et al., 2016b).

### 3.2.2. SIMPLISMA

To further examine the results on the μIR spectra, SIMPLISMA treatment was applied. This method is applied to the 293 spectra recorded for non-irradiated and irradiated samples by gamma, e-beam, and X-ray. The analysis gives a result corresponding to a pure spectrum of the main species; a reconstructed spectrum is sufficient to take into account in the data set (RRSSQ = 0.02). The concentration profile of the pure component is used to define the presence of that component in each spectrum analyzed. Profiles are obtained for each irradiation technology at different doses after processing data with SIMPLISMA.

The extracted spectrum represents the EVA spectrum (Fig. S1 in SI), involve 98% of the species present in the spectra analyzed by μIR on the cross-section. The narrow thickness of the EVOH layer (5 μm) does not allow its analysis by this technique. The μIR method supports the conclusion that there is no modification of the EVA layer in the multilayer film after irradiation by gamma, X-ray, or e-beam radiation at a dose below 100 kGy.

### 3.3. UV–visible spectroscopy (UV–Vis)

Fig. 7b displays the UV–Vis spectra of multilayer EVA/EVOH/EVA film non-irradiated and irradiated at 50 and 100 kGy by gamma, e-beam and X-ray radiation.

The spectra of non-irradiated and irradiated films are different (Fig. 7), it can be due to radiation affects the antioxidants present in samples (Tao et al., 2020). For the three irradiation technologies, the UV–Vis band present on the spectrum between 250 and 300 nm (Fig. 7) is similar, but the intensity of this band differs between gamma, e-beam and X-ray.

The aim of the PLS model is to extrapolate the effect of irradiation on the EVA/EVOH/EVA film, to know the radiation absorbed dose to the polymers regardless of the irradiation technologies. We performed three PLS models, one for each irradiation technology.

For the three PLS models, half of the non-irradiated samples and all of the 30 and 60 kGy irradiated samples were used. Samples irradiated at 45 kGy and half of the non-irradiated samples are used for prediction. The model was then used to predict the dose absorbed by samples irradiated by two other irradiations at 30, 45 and 60 kGy (Table S3 in SI).

#### 3.3.1. Gamma irradiation partial least square model

The first model calibration is based on the UV–Vis spectra of samples irradiated by gamma. The modelling results ($R^2$ = 0.99, RMSEC = 3.03) show that a good correlation is obtained between the UV–Vis spectra and the absorbed gamma dose. The prediction results show that the model is applicable: the dose of non-irradiated samples is predicted with an average dose of 0 kGy, and the dose of samples irradiated by gamma at 44 kGy is predicted with an average dose of 43 kGy (Fig. 8). The model was then used to predict the dose received for samples irradiated by X-ray at 30,45, 60 and 100 kGy or e-beam at 30, 45 and 60 kGy. The results show that X-ray and e-beam doses are underestimated.

#### 3.3.2. X-ray partial least square model

The second model (Fig. 9) is based on the UV–Vis spectra of samples irradiated by X-ray, the modelling results ($R^2$ = 0.97, RMSEC = 7.1) show that a good correlation is obtained between the UV–Vis spectra and the X-ray dose absorbed. The prediction results show that the model is applicable: the dose of non-irradiated samples is predicted with an average dose of 3 kGy, and the dose of samples irradiated at 45 kGy is predicted at 45 kGy. The model was then used to predict the dose received for samples irradiated by gamma or e-beam at 30, 45 and 60 kGy. The results show that gamma doses are correctly predicted while e-beam doses are underestimated.

#### 3.3.3. e-beam partial least square model

The model (Fig. 10) is based on the UV–Vis spectra of samples irradiated by e-beam, the modelling results ($R^2$ = 0.99, RMSEC = 2.31) show that a good correlation is obtained between the UV–Vis spectra and the e-beam dose absorbed. The prediction results show that the model is applicable: The dose of non-irradiated samples predicted with an average dose of −1 kG y, and the dose of samples irradiated by e-beam at 47 kGy is predicted at 47 kGy. The model was then used to predict the dose received for samples irradiated by gamma or X-ray at 30, 45 and 60 kGy. The results show that gamma and X-ray are overestimated.

The three loadings (Fig. 11) represent the wavelength most correlated to the irradiation doses in each PLS model. The representation of the loadings differs according to the irradiation technology. As already explained in FTIR-ATR section, the gamma and the X-ray impact prediction are in good agreement certainly due to the fact dose rate are quite similar. The extend of the by-product concentration could be different. Their identification is provided in another reference (Dorey et al., 2020).

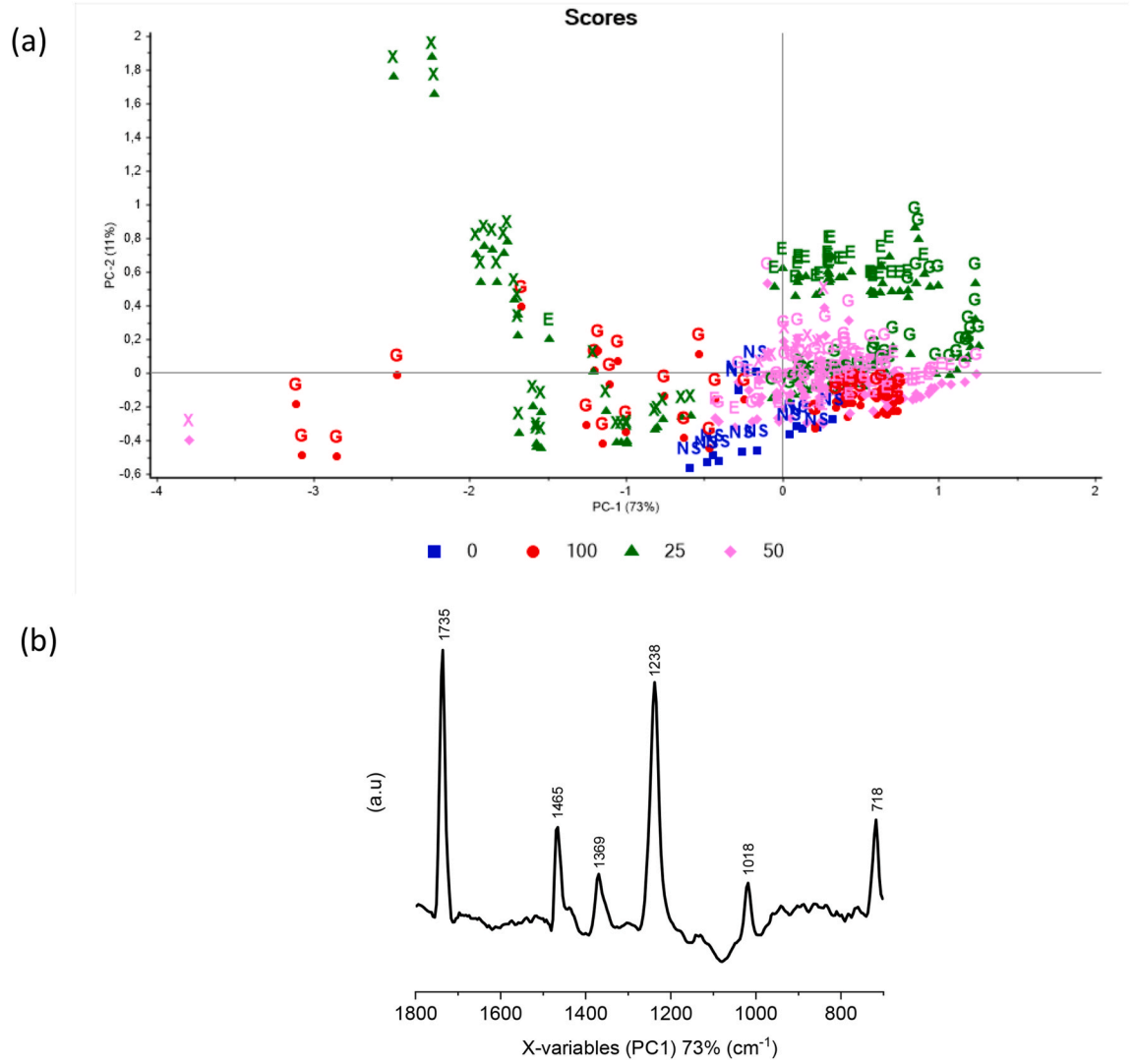


**Fig. 6.** PCA of 293 EVA spectra of non-irradiated and gamma, e-beam and X-ray irradiated samples at 25, 50 et 100 ± 10%. Spectra are baseline corrected and normalized. (a) Score plot of PCA with dose labels (b) Loading plot of PC1. G, X, E, NS stand for gamma, X-ray, e-beam, non-sterile respectively. The peak at 1737 $cm^{-1}$ corresponds to the $\nu$CO of the ester. Peaks included between 1470 and 1360 $cm^{-1}$ correspond to the deformation in the plane of the $\delta CH_2$ and $\delta CH_3$ groups. Peaks included between 1300 and 1020 $cm^{-1}$ correspond to the stretching $\nu$CO, and the peak at 719 $cm^{-1}$ corresponds to the inner rocking vibration of $CH_2$ in the amorphous part ($\delta CH_2$).

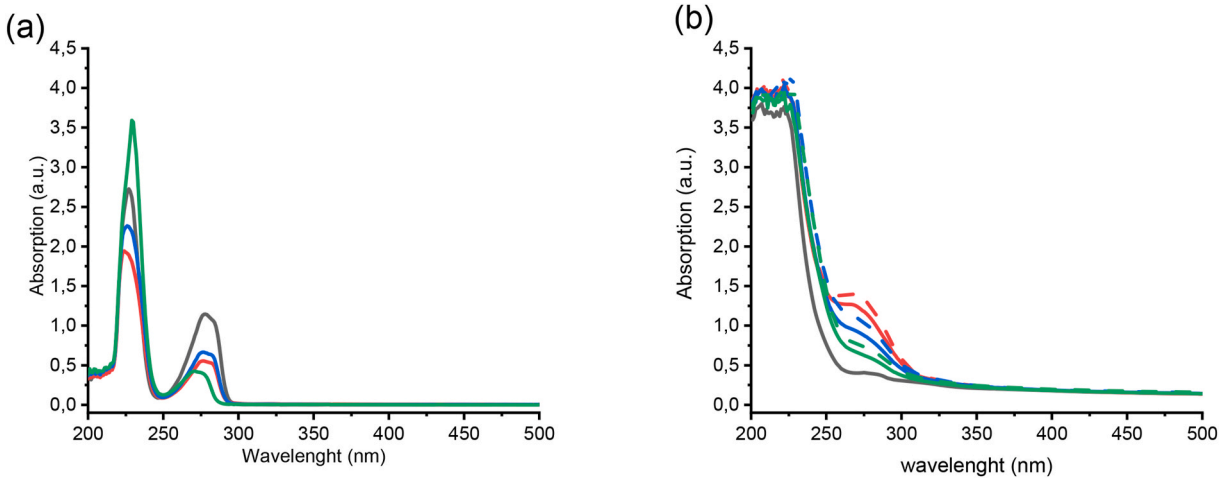


**Fig. 7.** (a) UV–Vis spectra of antioxidants dissolved in DCM: BHT (black line), Irganox® 1076 (red line), Irganox® 1010 (blue line) and Irgafos® 168 (green line). (b) Multilayer film non irradiated (black line), irradiated at 50 kGy (solid line) and 100 kGy (dotted line) by gamma (red line), X-ray (green line) and e-beam (blue line).

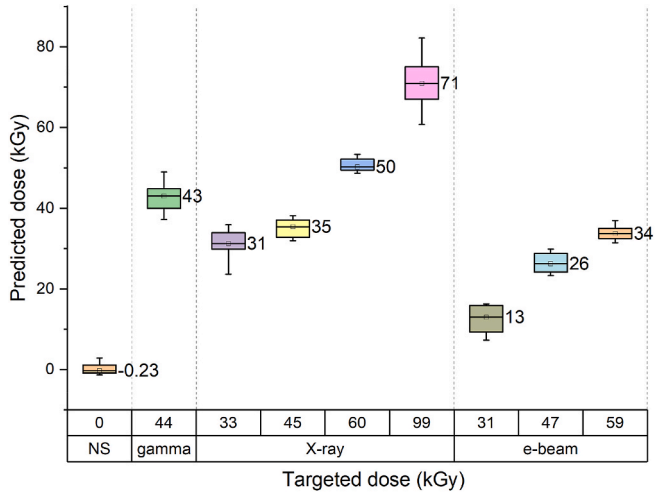


**Fig. 8.** (a) PLS model using UV spectra of gamma irradiated samples. Labels correspond to predicted doses. Missing data were used to build models: Non irradiated samples and samples irradiated at 30 and 60 kGy ± 10%.

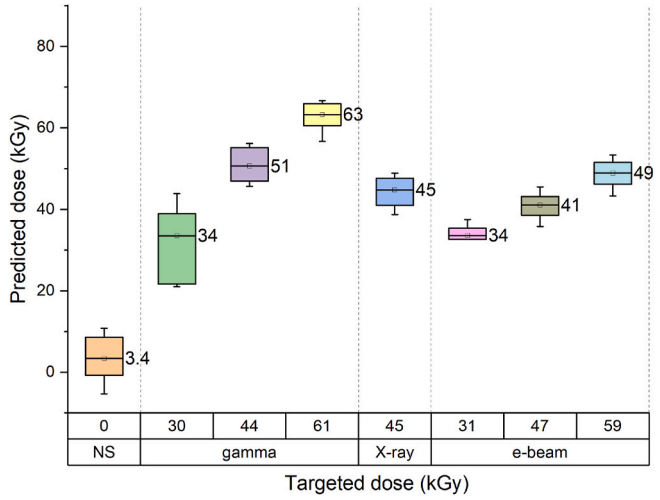


**Fig. 9.** PLS model using UV–Vis spectra of X-ray irradiated samples. Labels correspond to predicted doses. Missing data were used to build models. Non irradiated samples and samples irradiated at 30,60 and 100 kGy ± 10%.

## 4. Conclusions

The multilayer film composed of EVA/EVOH/EVA underwent analysis subsequent to gamma, e-beam, and X-ray irradiation at various scales. The analysis was conducted at a $cm^2$ scale using UV–Vis analysis, at a $mm^2$ scale using infrared analysis, and at a few $\mu m^2$ scale using micro infrared method.

The utilization of micro-infrared analysis does not discern the varying effects of the three irradiation technologies on polymers.

The feasibility of estimating the absorbed dose of a multilayer film can be achieved through UV–Vis or FTIR analysis of the impact of irradiation on the film, given a predetermined irradiation dose. Nonetheless, the extrapolation of the absorbed dose modelling is not universally applicable to all irradiation technologies. The estimation of absorbed dose in e-beam irradiated films is undervalued when projected from models based on gamma or X-ray. The impact of e-beam irradiation, as assessed through UV–Vis and FTIR analysis, differs from that of gamma and X-ray irradiation on the multilayer film.

Both gamma ray and X-ray exhibit comparable effects on the multilayer film, and it is feasible to anticipate the absorbed dosage of the film by utilizing UV–Vis spectra or infrared spectra for gamma ray or X-ray of a predetermined dose. The modifications after gamma and X-ray irradiations are close to the methodology detection capability, revealing the modifications happen in low extent.

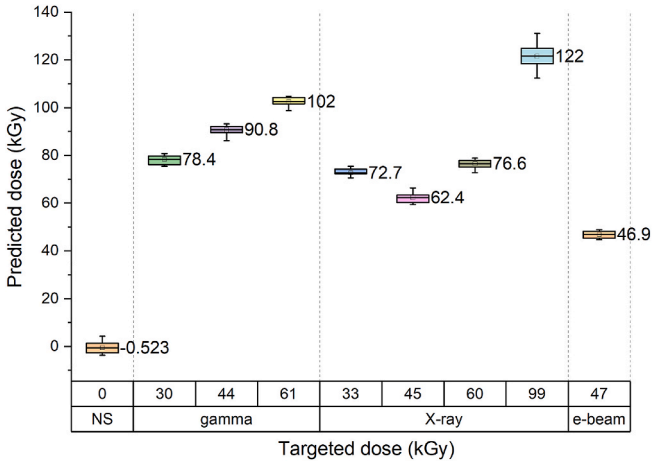


**Fig. 10.** PLS model using UV–Vis spectra of e-beam irradiated samples. Labels correspond to predicted doses. Missing data were used to build models. Non irradiated samples and samples irradiated at 30 and 60 kGy ± 10%.

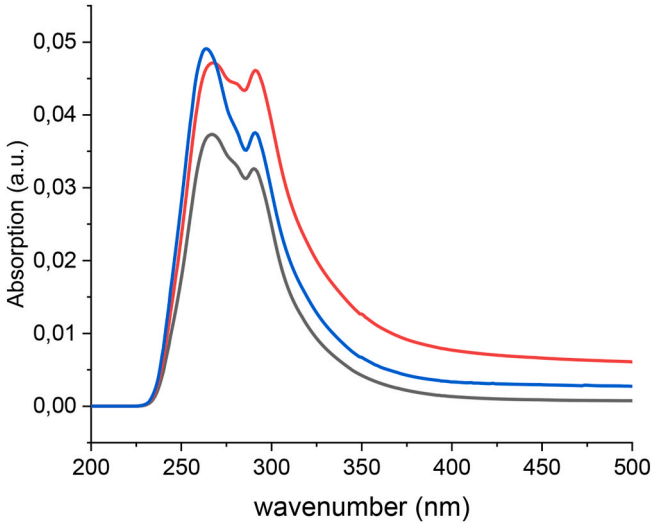


**Fig. 11.** Loading of the UV–Vis spectra of EVA/EVOH/EVA film irradiated by gamma (black line), e-beam (blue line) and X-ray (red line).

## Funding

Support for PNNL participation in this research was provided by the USDOE National Nuclear Security Administration Office of Radiological Security.

## CRediT authorship contribution statement

**Blanche Krieguer:** Data curation, Investigation, Methodology, Validation, Visualization, Writing – original draft, Writing – review & editing. **Sylvain R.A. Marque:** Conceptualization, Data curation, Funding acquisition, Investigation, Methodology, Project administration, Resources, Supervision, Validation, Visualization, Writing – review & editing. **Samuel Dorey:** Conceptualization, Data curation, Funding acquisition, Investigation, Methodology, Project administration, Resources, Supervision, Validation, Visualization, Writing – review &

editing. **Fabien Girard:** Conceptualization, Data curation, Funding acquisition, Investigation, Methodology, Project administration, Resources, Supervision, Validation, Visualization, Writing – review & editing. **Yelin Ni:** Formal analysis, Investigation, Methodology, Validation, Visualization, Writing – review & editing. **Donghui Li:** Formal analysis, Methodology, Validation, Visualization, Writing – review & editing. **Mark K. Murphy:** Conceptualization, Data curation, Funding acquisition, Investigation, Methodology, Project administration, Resources, Supervision, Validation, Visualization, Writing – review & editing. **Leonard S. Fifield:** Conceptualization, Data curation, Funding acquisition, Investigation, Methodology, Project administration, Resources, Supervision, Validation, Visualization, Writing – review & editing. **Nathalie Dupuy:** Conceptualization, Data curation, Funding acquisition, Investigation, Methodology, Project administration, Resources, Supervision, Validation, Visualization, Writing – review & editing.

## Declaration of competing interest

The authors declare the following financial interests/personal relationships which may be considered as potential competing interests: Samuel Dorey reports equipment, drugs, or supplies, statistical analysis, and writing assistance were provided by Sartorius Stedim FMT SAS.

## Data availability

The data that has been used is confidential.

## Acknowledgements

We acknowledge Sartorius Stedim FMT S.A.S for the financial support of this work. N. D, F.G and S.R.A.M are thankful to AMU and CNRS for support. We acknowledge Nina Girard-Perier for her technical assistance. The Pacific Northwest National Laboratory (PNNL) is operated by Battelle for the U.S. Department of Energy (USDOE) under Contract DE-AC05-76RL01830.

## Appendix A. Supplementary data

Supplementary data to this article can be found online at https://doi.org/10.1016/j.radphyschem.2024.111607.

## References

Ahmed, J., Wu, J., Mushtaq, S., Zhang, Y., 2020. Effects of electron beam irradiation and multi-functional monomer/co-agents on the mechanical and thermal properties of ethylene-vinyl acetate copolymer/polyamide blends. Mater. Today Commun. 23, 100840 https://doi.org/10.1016/j.mtcomm.2019.100840.

Armenante, P.M., Akiti, O., 2019. Sterilization processes in the pharmaceutical industry. In: am Ende, D.J., am Ende, M.T. (Eds.), Chemical Engineering in the Pharmaceutical Industry. John Wiley & Sons, Inc., Hoboken, NJ, USA, pp. 311–379. https://doi.org/10.1002/9781119600800.ch64.

Audran, G., Dorey, S., Dupuy, N., Gaston, F., Marque, S.R.A., 2015. Degradation of γ-irradiated polyethylene-ethylene vinyl alcohol-polyethylene multilayer films: an ESR study. Polym. Degrad. Stabil. 122, 169–179. https://doi.org/10.1016/j.polymdegradstab.2015.10.021.

Chmielewski, A.G., Sun, Y. (Eds.), 2017. Applications of Ionizing Radiation in Materials Processing, vol. 1. Institute of Nuclear Chemistry and Technology, Warszawa.

Darwis, D., Erizal, Abbas, B., Nurlidar, F., Putra, D.P., 2015. Radiation processing of polymers for medical and pharmaceutical applications. Macromol. Symp. 353, 15–23. https://doi.org/10.1002/masy.201550302.

Daszykowski, M., Kaczmarek, K., Vander Heyden, Y., Walczak, B., 2007. Robust statistics in data analysis — a review. Chemometr. Intell. Lab. Syst. 85, 203–219. https://doi.org/10.1016/j.chemolab.2006.06.016.

Di Benedetto, D., Breuil, P., 2007. Spectrophotométrie d'absorption dans l'ultraviolet et le visible. Tech. Anal. https://doi.org/10.51257/a-v2-p2795.

Dinesh, M., Chikkakuntappa, R., 2013. Microwave irradiation induced modifications on the interfaces in SAN/EVA/PVC and PVAc/BPA/PVP ternary polymer blends: positron lifetime study. Nucl. Instrum. Methods Phys. Res. Sect. B Beam Interact. Mater. Atoms 310, 67–74. https://doi.org/10.1016/j.nimb.2013.05.020.

Dorey, S., Gaston, F., Girard-Perier, N., Dupuy, N., Marque, S.R.A., Barbaroux, M., Audran, G., 2020. Identification of chemical species created during γ-irradiation of antioxidant used in polyethylene and polyethylene- *co* -vinyl acetate multilayer film. J. Appl. Polym. Sci. 137, 49336 https://doi.org/10.1002/app.49336.

Driffield, M., Bradley, E.L., Leon, I., Lister, L., Speck, D.R., Castle, L., Potter, E.L.J., 2014. Analytical screening studies on irradiated food packaging. Food Addit. Contam. 31, 556–565. https://doi.org/10.1080/19440049.2013.865087.

Dupuy, N., Marque, S.R.A., Fifield, L.S., Pharr, M., Staack, D., Pillai, S.D., Nichols, L., Murphy, M.K., Dorey, S., 2022. Supplementing gamma sterilization with X-ray and E-beam technologies. Bioproc. Technol. 20, 24–28.

Entezam, M., Aghjeh, M.K.R., Ghaffari, M., 2017. Electron beam irradiation induced compatibilization of immiscible polyethylene/ethylene vinyl acetate (PE/EVA) blends: mechanical properties and morphology stability. Radiat. Phys. Chem. 131, 22–27. https://doi.org/10.1016/j.radphyschem.2016.10.016.

Ergon, R., Esbensen, K.H., 2002. PCR/PLSR optimization based on noise covariance estimation and Kalman filtering theory. J. Chemom. 16, 401–407. https://doi.org/10.1002/cem.732.

Fifield, L.S., Pharr, M., Staack, D., Pillai, S.D., Nichols, L., McCoy, J., Faucette, T., Bisel, T.T., Huang, M., Hasan, M.K., Perkins, L., Cooley, S.K., Murphy, M.K., 2021. Direct comparison of gamma, electron beam and X-ray irradiation effects on single-use blood collection devices with plastic components. Radiat. Phys. Chem. 180, 109282 https://doi.org/10.1016/j.radphyschem.2020.109282.

Gardette, J.-L., 1998. Caractérisation des polymères par spectrométrie optique.

Gaston, F., Dupuy, N., Marque, S.R.A., Barbaroux, M., Dorey, S., 2016a. FTIR study of ageing of γ-irradiated biopharmaceutical EVA based film. Polym. Degrad. Stabil. 129, 19–25. https://doi.org/10.1016/j.polymdegradstab.2016.03.040.

Gaston, F., Dupuy, N., Marque, S.R.A., Barbaroux, M., Dorey, S., 2016b. One year monitoring by FTIR of γ-irradiated multilayer film PE/EVOH/PE. Radiat. Phys. Chem. 125, 115–121. https://doi.org/10.1016/j.radphyschem.2016.03.010.

Gaston, F., Dupuy, N., Marque, S.R.A., Dorey, S., 2018. Evaluation of multilayer film stability by Raman spectroscopy after gamma-irradiation sterilization process. Vib. Spectrosc. 96, 52–59. https://doi.org/10.1016/j.vibspec.2018.03.002.

Gemperline, P.J., 1989. Mixture analysis using factor analysis I: calibration and quantitation. J. Chemom. 3, 549–568. https://doi.org/10.1002/cem.1180030404.

Girard-Perier, N., Dorey, S., Gaston, F., Girard, F., Marque, S.R.A., Dupuy, N., 2022a. One-year ageing FTIR monitoring of PE/EVOH/PE film after gamma or electron beam irradiation. Polym. Degrad. Stabil. 195, 109790 https://doi.org/10.1016/j.polymdegradstab.2021.109790.

Girard-Perier, N., Marque, S.R.A., Dupuy, N., Claeys-Bruno, M., Gaston, F., Dorey, S., Fifield, L.S., Ni, Y., Li, D., Fuchs, W.K., Murphy, M.K., Pillai, S.D., Pharr, M., Nichols, L., 2022b. Effects of X-rays, electron beam, and gamma irradiation on chemical and physical properties of EVA multilayer films. Front. Chem. 10, 888285 https://doi.org/10.3389/fchem.2022.888285.

Hamilton, J.C., Gemperline, P.J., 1990. Mixture analysis using factor analysis. II: self-modeling curve resolution. J. Chemom. 4, 1–13. https://doi.org/10.1002/cem.1180040103.

Ji, Y.-Y., Chang, H.-S., Lim, T., Lee, W., 2019. Application of a SrI2(Eu) scintillation detector to in situ gamma-ray spectrometry in the environment. Radiat. Meas. 122, 67–72. https://doi.org/10.1016/j.radmeas.2019.01.014.

Komolprasert, V., 2016. Packaging food for radiation processing. Radiat. Phys. Chem. 129, 35–38. https://doi.org/10.1016/j.radphyschem.2016.07.023.

Kroc, T.K., 2023. Monte Carlo simulations demonstrating physics of equivalency of gamma, electron-beam, and X-ray for radiation sterilization. Radiat. Phys. Chem. 204, 110702 https://doi.org/10.1016/j.radphyschem.2022.110702.

Kumar, N., Bansal, A., Sarma, G.S., Rawal, R.K., 2014. Chemometrics tools used in analytical chemistry: an overview. Talanta 123, 186–199. https://doi.org/10.1016/j.talanta.2014.02.003.

Liang, Y.-Z., Kvalheim, O.M., 1996. Robust methods for multivariate analysis — a tutorial review. Chemometr. Intell. Lab. Syst. 32, 1–10. https://doi.org/10.1016/0169-7439(95)00006-2.

Martens, H., 1979. Factor analysis of chemical mixtures. Anal. Chim. Acta 112, 423–442. https://doi.org/10.1016/S0003-2670(01)85040-6.

Martens, H., Naes, T., 1989. Multivariate Calibration. Wiley.

Matsui, T., Shimoda, M., Osajima, Y., 1992. Mechanical changes of electron beam irradiated ethylene–vinyl acetate copolymer (EVA) film (I). Polym. Int. 29, 85–90. https://doi.org/10.1002/pi.4990290204.

Moondra, S., Raval, N., Kuche, K., Maheshwari, R., Tekade, M., Tekade, R.K., 2018. Sterilization of pharmaceuticals. In: Dosage Form Design Parameters. Elsevier, pp. 467–519. https://doi.org/10.1016/B978-0-12-814421-3.00014-2.

NicDaéid, N., 2018. Systematic drug identification. In: Reference Module in Chemistry, Molecular Sciences and Chemical Engineering. Elsevier, B9780124095472144579. https://doi.org/10.1016/B978-0-12-409547-2.14457-9.

Sjöström, M., Wold, S., Lindberg, W., Persson, J.-Å., Martens, H., 1983. A multivariate calibration problem in analytical chemistry solved by partial least-squares models in latent variables. Anal. Chim. Acta 150, 61–70. https://doi.org/10.1016/S0003-2670(00)85460-4.

Tao, B., Wang, G., Yin, Z., Pu, X., Jiang, Y., Zhang, L., Cheng, J., Li, Y., Zhang, J., 2020. Determination of the contents of antioxidants and their degradation products in sodium chloride injection for blood transfusion. J. Anal. Methods Chem. 2020, 1–12. https://doi.org/10.1155/2020/8869576.

Tarantili, P.A., Kiose, V., 2008. Effect of accelerated aging on the structure and properties of monolayer and multilayer packaging films. J. Appl. Polym. Sci. 109, 674–682. https://doi.org/10.1002/app.28091.

Valente, T.A.M., Silva, D.M., Gomes, P.S., Fernandes, M.H., Santos, J.D., Sencadas, V., 2016. Effect of sterilization methods on electrospun poly(lactic acid) (PLA) fiber alignment for biomedical applications. ACS Appl. Mater. Interfaces 8, 3241–3249. https://doi.org/10.1021/acsami.5b10869.

Voronko, Y., Chernev, B.S., Eder, G.C., 2014. Spectroscopic investigations on thin adhesive layers in multi-material laminates. Appl. Spectrosc. 68, 584–592. https://doi.org/10.1366/13-07291.

Windig, W., 1997. Spectral data files for self-modeling curve resolution with examples using the Simplisma approach. Chemometr. Intell. Lab. Syst. 36, 3–16. https://doi.org/10.1016/S0169-7439(96)00061-5.

Windig, W., 1994. The use of second-derivative spectra for pure-variable based self-modeling mixture analysis techniques. Chemometr. Intell. Lab. Syst. 23, 71–86. https://doi.org/10.1016/0169-7439(93)E0058-C.

Windig, W., Stephenson, D.A., 1992. Self-modeling mixture analysis of second-derivative near-infrared spectral data using the SIMPLISMA approach. Anal. Chem. 64, 2735–2742. https://doi.org/10.1021/ac00046a015.

Windig, Willem, Guilment, Jean, 1991. Interactive self-modeling mixture analysis. Anal. Chem. 63, 1425–1432. https://doi.org/10.1021/ac00014a016.

Wool, R.P., Bretzlaff, R.S., Li, B.Y., Wang, C.H., Boyd, R.H., 1986. Infrared and Raman spectroscopy of stressed polyethylene. J. Polym. Sci., Part B: Polym. Phys. 24, 1039–1066. https://doi.org/10.1002/polb.1986.090240508.

Wrobel, T.P., Vichi, A., Baranska, M., Kazarian, S.G., 2015. Micro-attenuated total reflection fourier transform infrared (micro ATR FT-IR) spectroscopic imaging with variable angles of incidence. Appl. Spectrosc. 69, 1170–1174. https://doi.org/10.1366/15-07963.